
CHALMERS
UNIVERSITY OF TECHNOLOGY

# Effect of processing gas on spatter generation and oxidation of TiAl6V4 alloy in laser powder bed fusion process

Applied Surface Science 613 (2023) 156089

Contents lists available at ScienceDirect

Applied Surface Science

journal homepage: www.elsevier.com/locate/apsusc

Full Length Article

# Effect of processing gas on spatter generation and oxidation of TiAl6V4 alloy in laser powder bed fusion process

Ahmad Raza [a,*], Camille Pauzon [a,b], Sophie Dubiez-Le Goff [c], Eduard Hryha [a]

[a] Chalmers University of Technology, Department of Industrial and Materials Science, SE-41296 Göteborg, Sweden
[b] Université Grenoble Alpes, CNRS, Grenoble INP, SIMaP, 38000 Grenoble, France
[c] Linde AG AT EMEA, Carl-von-Linde-Straße 25, DE-85716 Unterschleißheim, Germany

ARTICLE INFO

*Keywords:*
Powder degradation
Spatters formation
Surface analysis
Powder reusability
XPS
TiAl6V4

ABSTRACT

The atmosphere is a vital factor influencing powder degradation during laser powder bed fusion. Particularly, its purity, density, and thermal conductivity, can strongly affect spatter generation, thermal history, and oxidation. It is critical to understand the atmosphere-spatter properties relationship to enhance powder recyclability and overall process sustainability. Herein, the effect of processing gases, among pure Ar, (Ar+He), and He, on spatter generation and oxidation during TiAl6V4 processing is investigated. To evaluate their influence on impurity pickup and morphology of spatters, bulk chemical analysis and scanning electron microscopy were conducted. The nature and thickness of surface oxides on spatters were comprehensively examined using surface analysis tools including X-ray photoelectron spectroscopy, Auger electron spectroscopy, and nano secondary ion mass spectroscopy. The bulk chemical analysis showed a 70% increase in oxygen content and a 3-fold increase in nitrogen content from virgin to spatter collected in standard argon atmosphere. The increase of impurities was substantially lower for the spatters generated in He and the mixture of (Ar+He). The surface analysis showed that the spatter surface was covered with a uniform Ti- and Al-rich oxide layer along with Al-based oxide particulates. Finally, this study discusses the nature of oxide on TiAl6V4 spatters.

## 1. Introduction

Powder bed fusion-laser beam (PBF-LB) is a powder-based additive manufacturing (AM) technique, that has gained a lot of attention both from the industry and research community owing to the possibility to produce near-net-shape products with better design accuracy. Being an emerging field, PBF-LB still must counter various challenges for vast adaptability in the manufacturing industry. One such challenge is the reusability of unconsumed powder after each build to reduce the cost and increase the sustainability of the process. However, accumulated impurities and powder oxidation during processing can degrade the quality of powder compared to its virgin state and affect the reproducibility and properties consistency in fabricated parts by introducing defects [1]. Recently, several research studies have discussed the powder degradation mechanism in the PBF-LB process [2–4]. During PBF-LB, spatter generation and accumulation in unconsumed powder is the dominant powder degradation mechanisms [5,6].

Spatters are unavoidable by-products of the PBF-LB process which are generated during the laser-melt-powder interaction [7–9]. Based on spatters origin, spatters can be molten/partially molten, hot, or cold [10]. As the PBF-LB process is usually conducted in an inert atmosphere with 1000 ppm residual oxygen, spatters can interact with this residual oxygen and get oxidized [11,12]. A non-negligible amount of oxidized spatter will have a size like feedstock powder and will be retained in reused powder upon sieving [13,14]. Accumulation of such spatters in the powder bed can be detrimental to the properties of fabricated parts. A study conducted on the reusability of AlSi10Mg powder for 30 months (5000 machine hours) showed that the number of extremely oxidized spatter particles reached above 3 % after 30 months of reuse, even though the powder was refurbished with the addition of virgin powder to compensate the consumed powder [15]. A subsequent study, and a few other investigations regarding the effect of powder reuse showed an increase in porosity and degradation of mechanical properties [16,17]. Another investigation on HX alloy showed that the presence of spatters can increase the occurrence of stochastic flaws by creating a lack of fusion defects stemming from the oxidized surface of spatter particles [18]. Hence, it is important to reduce the extent of spatter generation and oxidation to decrease the rate of powder degradation.

* Corresponding author.
*E-mail address:* ahmadra@chalmers.se (A. Raza).

https://doi.org/10.1016/j.apsusc.2022.156089
Received 16 August 2022; Received in revised form 3 December 2022; Accepted 12 December 2022
Available online 16 December 2022

The generation of spatters is influenced by process parameters such as laser power, scan speed, layer thickness, and part geometry. The laser power and scan speed determines the temperature of melt pool and regulates the evaporation and recoil pressure. Higher laser power and lower scan speed result in greater energy input and resultantly are typically associated with a generation of a high volume of spatters [19–21]. Moreover, the studies using in-situ monitoring systems have showed that the number of hot incandescent spatters increases with the powder layer thickness. Lastly, Chen et al. studied the effect of part geometry using lattice structures on the spatter generation and found that the lattices with higher thickness and larger overhang structures increase the generation of spatters [22].

Purity and nature of processing gas can assist in reducing the extent of spatter generation and oxidation. A recent study by Raza et al. on Alloy 718 investigated the effect of residual oxygen on the extent of spatter oxidation and found that the purity of the atmosphere from 1000 ppm to 20 ppm residual oxygen content can reduce the oxygen pickup by 70 % [23]. On an associated note, a study by Amano et al. [24] showed that the decrease in residual oxygen content in the build chamber can reduce the number of generated spatters. Furthermore, the studies regarding the effect of processing gas on spatter formation have shown that the use of He can reduce the extent of spatter generation compared to Ar gas while processing TiAl6V4 alloy [24–26]. The reduced number of spatters in He atmosphere has been attributed to the 10-fold higher thermal conductivity of the He compared to the Ar gas [27]. However, there is still a lack of understanding regarding the influence of processing atmosphere on the extent of spatter oxidation.

In this study, the effect of atmospheric gas on the formation and oxidation of the spatter particles during the processing of TiAl6V4 alloy is investigated. Three variations of gases have been employed including Ar, He, and a mixture of both named ADDvance® Laser230. A comprehensive surface analysis using XPS, AES and NanoSIMS is conducted to compare the spatter surface properties. This is further complemented by microscopy and bulk chemical analysis.

## 2. Materials and methods

Fresh plasma atomised Ti6Al4V powder (AP&C, GE Additive) was used as feedstock material and was processed in an EOS M290 (EOS GmbH) PBF-LB machine. The particle size distribution measured by laser diffraction with a Mastersizer 3000 (Malvern Panalytical) was characterized by a $D_{10}$ of 23 μm, $D_{50}$ of 33 μm and $D_{90}$ of 48 μm (average values obtained from 5 measurements). The build jobs conducted were identical and conducted under three high purity atmospheres with less than 40 ppm impurities: pure Ar, pure He, and a mixture of Ar and He under the commercial name ADDvance® Laser230 by Linde AG, as described in details elsewhere [28]. The properties of these gases are presented in Table 1. For each process atmosphere, the oxygen control system was calibrated with reference calibration gases of similar composition. For example, for the He-based build job, a He calibration gas was employed with oxygen impurity level close to the residual oxygen expected during printing. In addition, other variables such as gas speed of 2–2.2 m/s, build job layout, laser process parameters were kept unchanged between jobs, and the TiAl6V4 powder was not recycled.

The total build time was about 15 h under each atmosphere, and it corresponds to the duration allowing to collect about >10 g of spatters in the standard Ar atmosphere. After both build jobs were completed, spatters were carefully collected at different positions in the build chamber, namely, on top of the gas inlet, on top of the gas outlet and in the gas outlet. The gas inlet and outlet are the apertures placed symmetrically on both sides of the build area, through which the process gas recirculates, as shown in Fig. 1. Our previous studies have shown that deposits gather on the gas inlet and outlet are spatter particles ejected by laser-melt-powder interaction [23].

The collected samples were weighted with a high precision scale. The oxygen, nitrogen and hydrogen content of the virgin powder and samples were then measured by combustion analysis using a LECO ONH835. The built parts composition was measured for 3 samples at 5 positions on the baseplate for each build job and the average and standard deviation are given in the results section. A field emission gun scanning electron microscope LEO Gemini 1550 (SEM) was used to analyze the morphology of the virgin powder and the collected spatter particles.

Finally, X-ray photoelectron spectroscopy (XPS) was conducted using ULVAC-PHI 5500. The monochromatic Al Kα X-ray source was used for the analysis. Powder samples for XPS analysis were mounted on 3 M tape, and the dimensions of the analysis area were 300 × 300 $\mu m^2$. Due to the large measurement area, XPS results represent a statistical

**Table 1**
List of gas properties employed in this work (internal data of Linde).

| Gas | Density ($kg/m^3$) | Specific heat capacity at constant pressure (J/(kg·K)) | Thermal conductivity at 25 °C (W/(m·K)) |
|---|---|---|---|
| Ar | 1.62 | 520 | 0.016 |
| ADDvance® Laser230 | 1.18 | 734 | 0.035 |
| He | 0.16 | 5190 | 0.142 |

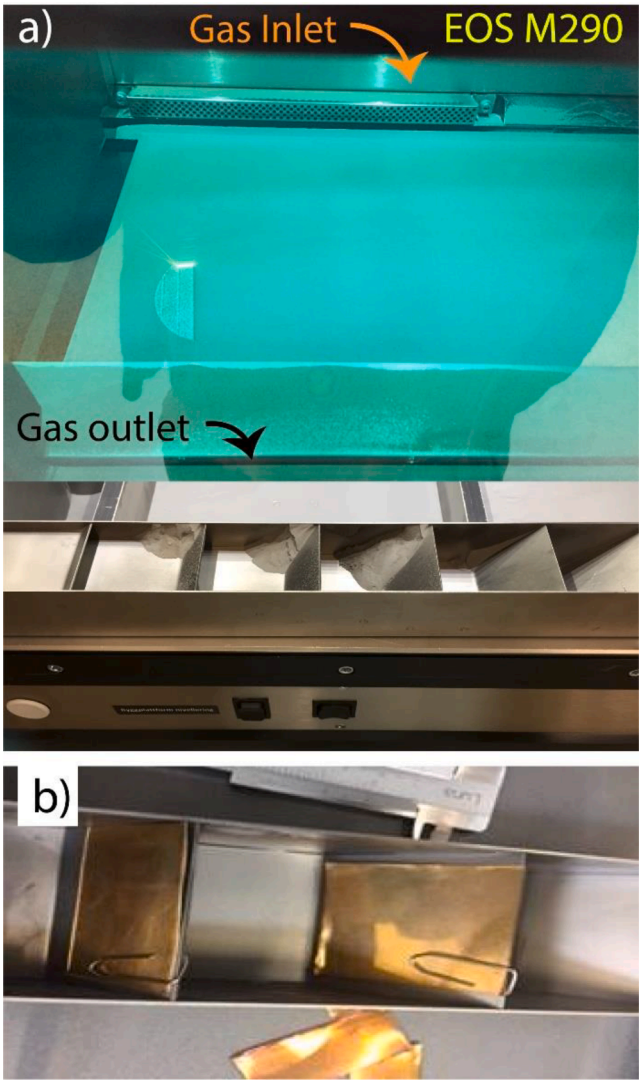


**Fig. 1.** The build chamber of the EOS M290 where a) is showing the gas inlet and outlet from where spatter samples were collected and b) is showing the gas outlet where Cu plates are placed to gather condensates.

average of about 20 to 30 particles. To avoid the charging effect due to insulated nature of template tape, continuous ion neutralization was done. Ar+ ion etching was done with an etch rate of ~5.2 nm/min to estimate the oxide layer thickness. The etch rate was calibrated using $TaO_2$ foil. The survey spectra and high-resolution narrow scans were acquired using a pass energy of 280 eV and 26 eV, respectively. The spectral analysis was conducted using MultiPak software provide by Physical Electronics. The peak shift was adjusted using C1s peak obtained from advantageous hydrocarbons at 284.8 eV.

Auger electron spectroscopy (AES) using a PHI 700 AES from Physical Electronics was done to further investigate the surface chemistry. The built-in SEM system assist in identifying the particle of interest and conducting surface analysis with a lateral resolution of up to 10 nm. The electron accelerating voltage was 10 kV and the beam current was 10nA, enabling a nominal analytical lateral resolution of 10 to 20 nm. Like XPS, $Ar^+$ ion etching was used to conduct the depth profile analysis and etch rate was 2.86 nm/min. The raster size for etching was 3 × 3 $mm^2$, and the voltage used was 2 kV. The etching rate was calibrated using $TaO_2$ foil. The samples were mounted on an Indium plate template to avoid surface damage on the sample surface and enhance the conductivity by using a metallic template. For avoiding the drift during analysis, the image registration was done, and position was recalibrated after every five cycles. The data analysis was done by using MultiPak Phi software provided by Physical Electronics.

Nano secondary ion mass spectroscopy (NanoSIMS) equipped with cesium ($Cs^+$) gun, by Cameca Nano-SIMS 50, France, with a spatial resolution of 50 nm was used to further analyze the surface of fresh powder and spatters. The data was collected by using multidetector mode by sputtering with 20*pA* $Cs^+$ primary ions. The field of view was 35 × 35 $\mu m^2$, and ES3, AS2 slits and D12 diaphragm were used during the analysis. The dwell time during the measurement was 1.5 ms. The samples were mounted on an Indium plate template for the analysis.

## 3. Results and discussion

### 3.1. Quantitative and chemical analysis of generated spatters

The effect of process gas on the amount of generated spatters in previous work [26] showed that the helium atmosphere can significantly reduce the number of generated incandescent spatters. Fig. 2 also shows a comparison between argon and ADDvance® Laser230 environment, where the introduction of He in Ar gas has reduced the quantity of incandescent spatters by 30 % with an Ar-He mixture. This highlights that the He environment allows to significantly decrease the quantity of spatters. The mechanism behind the reduction of spatters with the introduction of He gas in the build chamber has been comprehensively discussed by Pauzon et al. [26]. The trend towards reduction of spatters produced with additions of He to the process atmosphere seen in Fig. 2, is expected to be even more pronounced if a methodology to collect spatters directly from the powder bed would be established, based on the in situ observation of spatter generation in the following research works [26].

A bulk chemical oxygen analysis provides useful information concerning the extent of degradation both in the form of oxide formation and oxygen dissolution of the material. Oxygen, nitrogen, and hydrogen contents in virgin powder are 1679 ppm, 145, and 19 ppm, respectively. In comparison, spatters collected in the argon atmosphere show the highest increase in the contents of these elements with oxygen reaching 2710 ppm, which is a 70% increase from virgin powder. Besides that, nitrogen and hydrogen contents also increased 2–3 fold from virgin powder to spatters. An increase in ADDvance® Laser230 and helium samples is also significant but it is relatively lower than the argon sample. Hence, investigation of bulk chemical analysis shows that the use of both He and ADDvance® Laser230 can noticeably reduce the extent of degradation of spatter particles.

### 3.2. Morphology of spatters

The morphology of spatter samples obtained in different gas atmospheres is compared with that of the virgin powder, see Fig. 3. Overall particles have similar sphericity as the virgin powder, whereas the virgin powder has a surface free of any oxide particulates. On the other hand, the spatter particles' surface is covered with fine particulates. The morphology and coverage of such features is varying from argon atmosphere to ADDvance® Laser230 and helium. The particulates formed on spatters obtained from the argon atmosphere are coarser than in former atmospheres.

A closer look into the morphology of individual spatter particles highlights that not all have oxidized similarly. This is perhaps connected with the different origins of spatter particles. Fig. 4 shows three different spatter particles alongside their high magnification images where the difference in surface morphology is distinct. The particle in Fig. 4b has a morphology like the virgin powder with some nucleation of oxide particulates on the surface. However, oxidation and oxide particulate formation is more prevalent in the spatter particle shown in Fig. 4c. The surface of this spatter particle is fully covered with a granular oxide structure. Similar oxidation morphology was previously observed in spatters from AlSi10Mg alloy where the granular structure of oxide was coarser compared to this case [15]. The third type of spatter particles hints of recrystallization from the presence of fine martensitic substructure on the particles. Overall, the extent of oxidation and dominant oxides might be different in all three types of particles.

As the particles were collected from the gas outlet, there existed an ambiguity regarding the origin of oxide particulates formation on top of uniform Al-, Ti-based oxides layer. There is a need to elucidate the fact if these particles are grown by the diffusion of Al from the core of the particle and not originated from the deposition of condensates that were brought by processing gas from the build chamber and condensated on the spatter particles, deposited in the inlet. To understand the extent of the oxide condensation during PBF-LB of Ti64 in the outlet, Cu plates

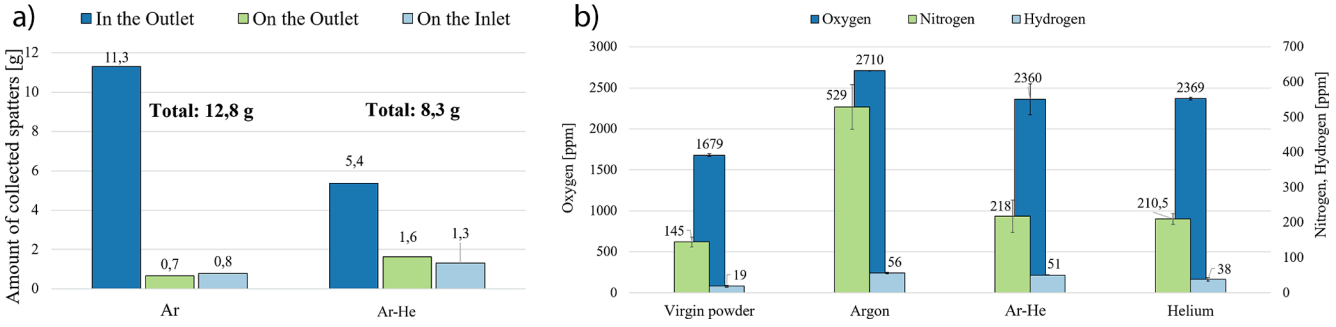


**Fig. 2.** a) Amount of collected spatters under Ar and Ar-He at the different locations: in the gas outlet, on the gas outlet and the gas inlet of the EOS M290, and b) O, N and H content of the virgin powder and spatter samples collected in the gas outlet, produced under Ar, Ar-He and He atmospheres.

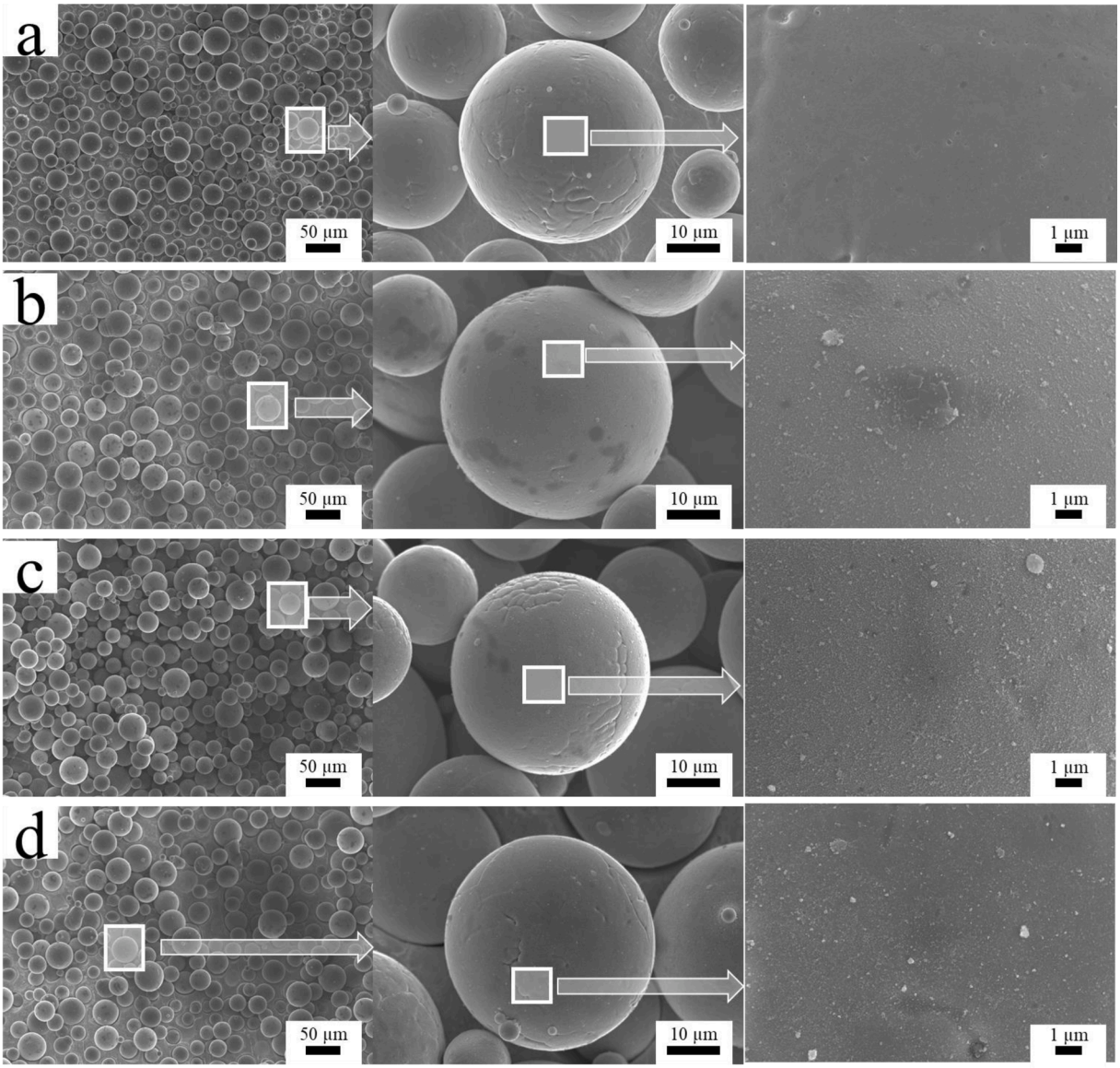


**Fig. 3.** Comparison of Ti6Al4V powder morphology of a) virgin powder sample, and spatter sample obtained during PBF-LB process in b) Ar, c) Ar-He mixture and d) He atmospheres.

were placed in the gas outlet during a 10 h build job, which is comparable to the build jobs from where spatter samples were collected, as shown in Fig. 1b. The SEM imaging of the Cu plate is shown in Fig. 5 where it is compared with a spatter particle with heavily oxidized and granular surface. The surface of the Cu plate and a spatter deposited on the plate is covered with condensates. The nature of these condensate particulates is fibrous with poor cohesion to the powder particle surface that is most probably removed during spatter handing and sieving. This is different from the oxide particulates formed on the surface of spatter particles, which are growing outwards. Moreover, the surface of spatters deposited in the gas outlet will be continuously shadowed by the incoming stream of spatters during build, and the spatters surface will not get as much time to collect condensate as the Cu plate got. This finding strengthens the assumption that oxide particulates formed on the spatter surface result from the internal diffusion of particles.

### 3.3. Surface analysis

#### 3.3.1. Powder surface oxide chemistry

XPS survey scan of the as-received surface of powder samples obtained in argon, ADDvance® Laser230, and helium atmospheres are shown in Fig. 6. The survey spectra for all the samples are not showing any distinguishable variation compared to that of the virgin powder. Distinct peaks of aluminium (Al2p), titanium (Ti2p), carbon (C1s), and oxygen (O1s) can be observed. The reason behind the similarity between virgin and spatter sample spectra is the formation of Al- and Ti-based stable and homogeneous oxide layers. However, only the N1s peak at 396eV highlights a difference which is in line with the bulk chemical analysis. The N1s peak showed a distinctive increase in intensity from virgin powder to spatter particles. This increase is more significant in the argon atmosphere.

Considering the presence of a uniform oxide layer presence both on virgin and reused powder, XPS depth profiling can assist in providing comprehensive information regarding the oxide nature and thickness. Fig. 7 is showing a comparison of the depth profile of Ti2p, Al2p, and O1s spectra from virgin powder with the spatters collected from all three different processing gas. For Ti2p spectra in virgin powder (Fig. 7a), at a 7.5 nm etch depth, a dominant metal peak ($Ti2p^{met}_{3/2}$) at 454.10 eV compared to oxide peak ($Ti2p^{4+}_{3/2}$) at 459 eV can be observed, which is overlapping with $Ti2p^{met}_{1/2}$ peak. However, such a dominant $Ti2p^{met}_{3/2}$ peak

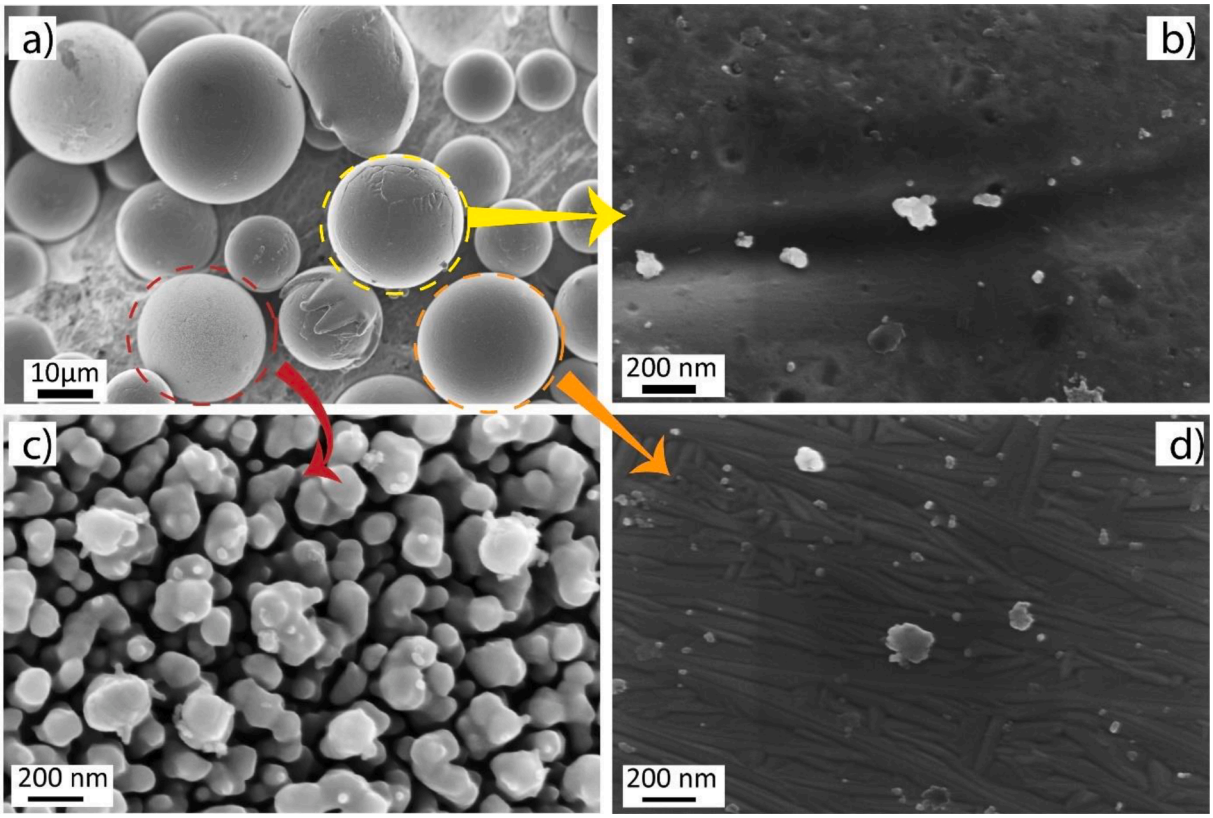


**Fig. 4.** SEM image analysis where a) shows collected spatter particles from Ar samples where b), c), and d) show high magnification image of individual particles.

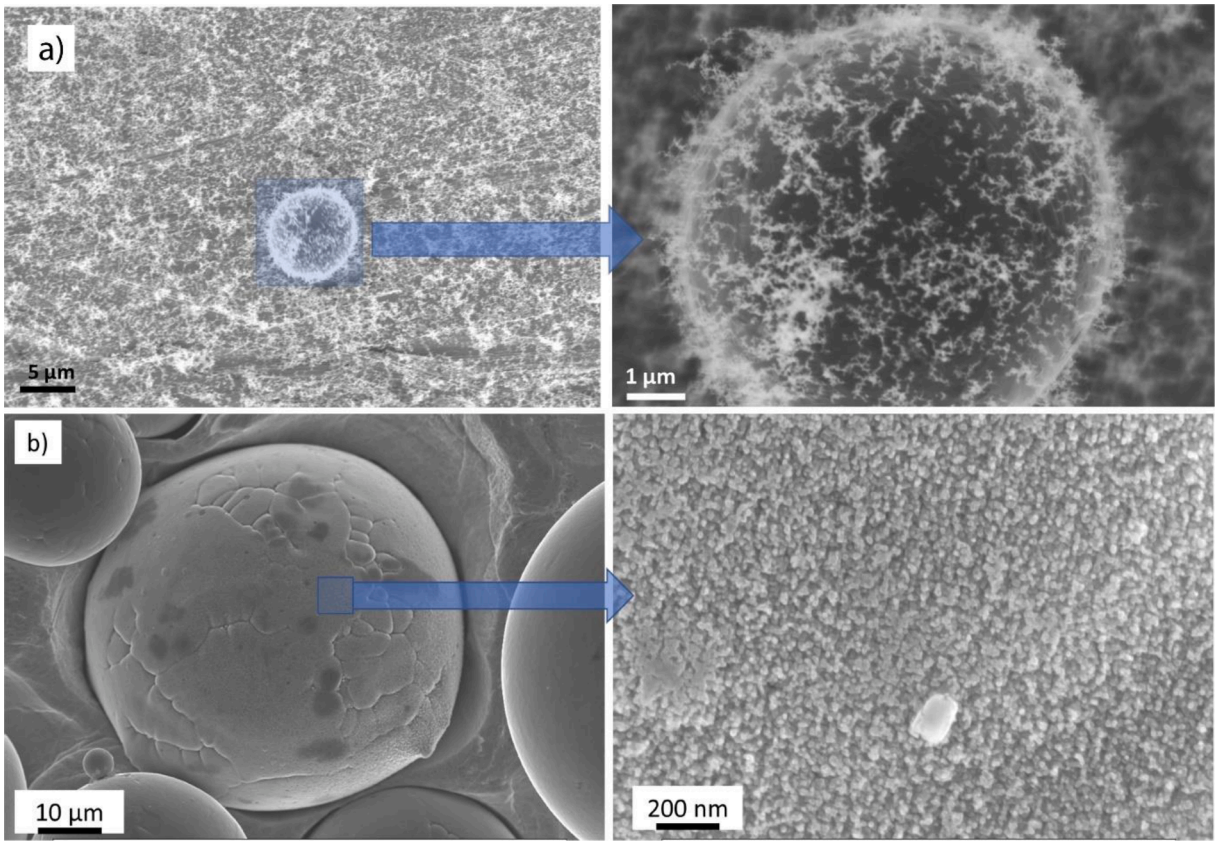


**Fig. 5.** A comparison of a) condensate deposition on Cu plate in the gas outlet and b) a spatter particle surface covered with oxide particulates.

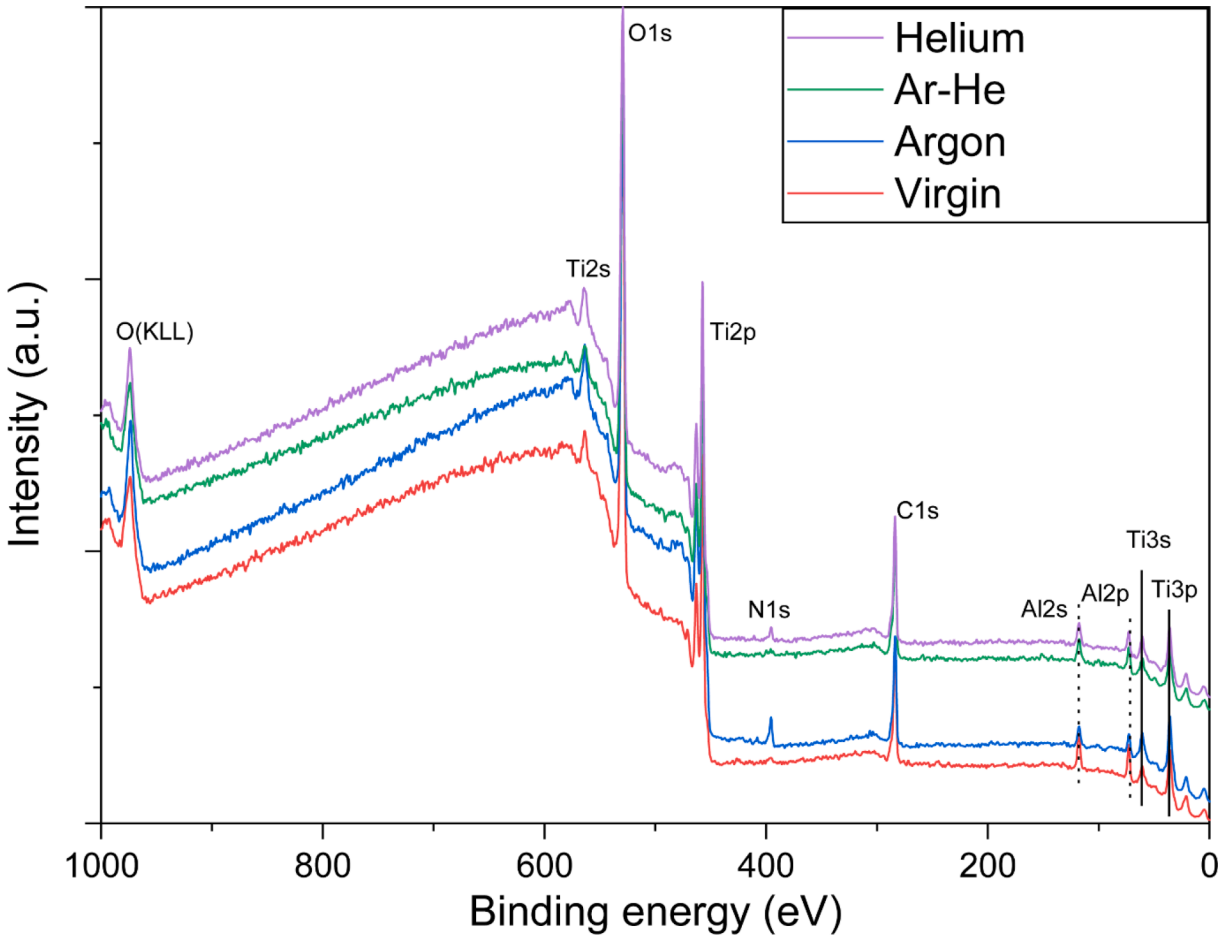


**Fig. 6.** XPS survey spectra of the virgin powder, of spatters generated under Ar, the Ar-He mixture and He atmospheres.

in spatters obtained from argon, ADDvance® Laser230, and helium was observed at 30 nm, 15 nm, and 15 nm etch depth respectively. This represents the thickening of the uniform oxide layer in spatters compared to virgin powder.

For Al2p spectra, an oxide peak ($Al2p^{3+}$) spectra can be observed at larger thicknesses compared to Ti2p. For example, a strong $Al2p^{3+}$ peak can be observed in Fig. 7b at the etch depth of 60 nm and disappeared between the etch depth of 60 nm and 150 nm. This indicates the presence of Al-rich oxide particulate formation. The thickness of such particulates is larger than uniform oxide layer thickness, which is the reason behind the appearance of $Ti2p^{met}_{3/2}$ at much lower etch depths. The comparison among spatter particles shows that the $Al2p^{3+}$ is persisting to the highest etch depth in the sample collected in argon followed by helium and ADDvance® Laser230. A comparison of O1s spectra also elucidates the drop in relative intensity is more sluggish in the sample from the argon atmosphere compared to all other samples. To summarize the data from depth profile analysis, the analysis has indicated that the spatters from the argon atmosphere have shown the highest oxidation compared to other samples.

Oxide-cation concentration w.r.t. depth profile calculation from XPS data can be useful in elucidating the dominant type of oxides and their thicknesses. Such calculation is done for Ti-oxide and Al-oxide cation and exhibited in Fig. 8 where a comparison between different samples as well as the type of oxides can be observed. In terms of spatter samples, the samples gathered from the argon atmosphere showed the presence of the highest amount of oxide cations of both Al- and Ti-, which is consistent even at larger etch depths. This is followed by helium and ADDvance® Laser230 environment, whereas, the virgin sample shows the least amount of oxide cations. Furthermore, the comparison of Ti- and Al-oxide cations shows that the thickness of Ti-oxide cations is shallower compared to the Al-oxide cations, which are prevalent at even larger etch depths. This prevalence perhaps originated from the particulate nature of Al-oxide which are coarser than the uniform Ti- and Al-oxide layer.

Normalized oxygen intensity w.r.t. etch depth provides information concerning the distribution of oxygen from the surface to the particle's core. Fig. 9a is showing a comparison of normalized oxygen intensities of all the above-mentioned samples. For the virgin sample, oxygen is mainly present just near the surface and disappeared after slight etching. However, in spatter, samples oxygen is present at a larger etch depths which is in line with the observed presence of Al-based oxide cations at larger etch depth. The normalized intensities of oxygen from the O1s spectra can be further used to estimate the oxide layer thickness [29,30]. The determined oxide layer thicknesses are in the units of $Ta_2O_5$ thickness units which were used to determine the etch rate during depth profiling. However, as investigated by Baer et al.[31] the etch rate of $Ta_2O_5$ is significantly different from the etch rate of $TiO_2$ and $Al_2O_3$, thus the actual values of oxide layer thickness will be substantially lower than the presented values here. By readjusting the measured oxide layer thickness following the comparison done by Baer et al., the actual oxide layer thickness will be ~ 7.2 nm, ~13.5 nm, ~11 nm, and 12 nm for the virgin powder, argon, ADDvance® Laser230 and helium spatter samples, respectively. Therefore, the oxide layer thickness of spatters obtained from the different atmospheric environments is slightly varying, however, connected with bulk oxygen content.

To summarize the findings from the comparison of microscopy and surface analysis of spatters from different gas atmospheres, the introduction of He in the atmosphere reducing the extent of oxidation of

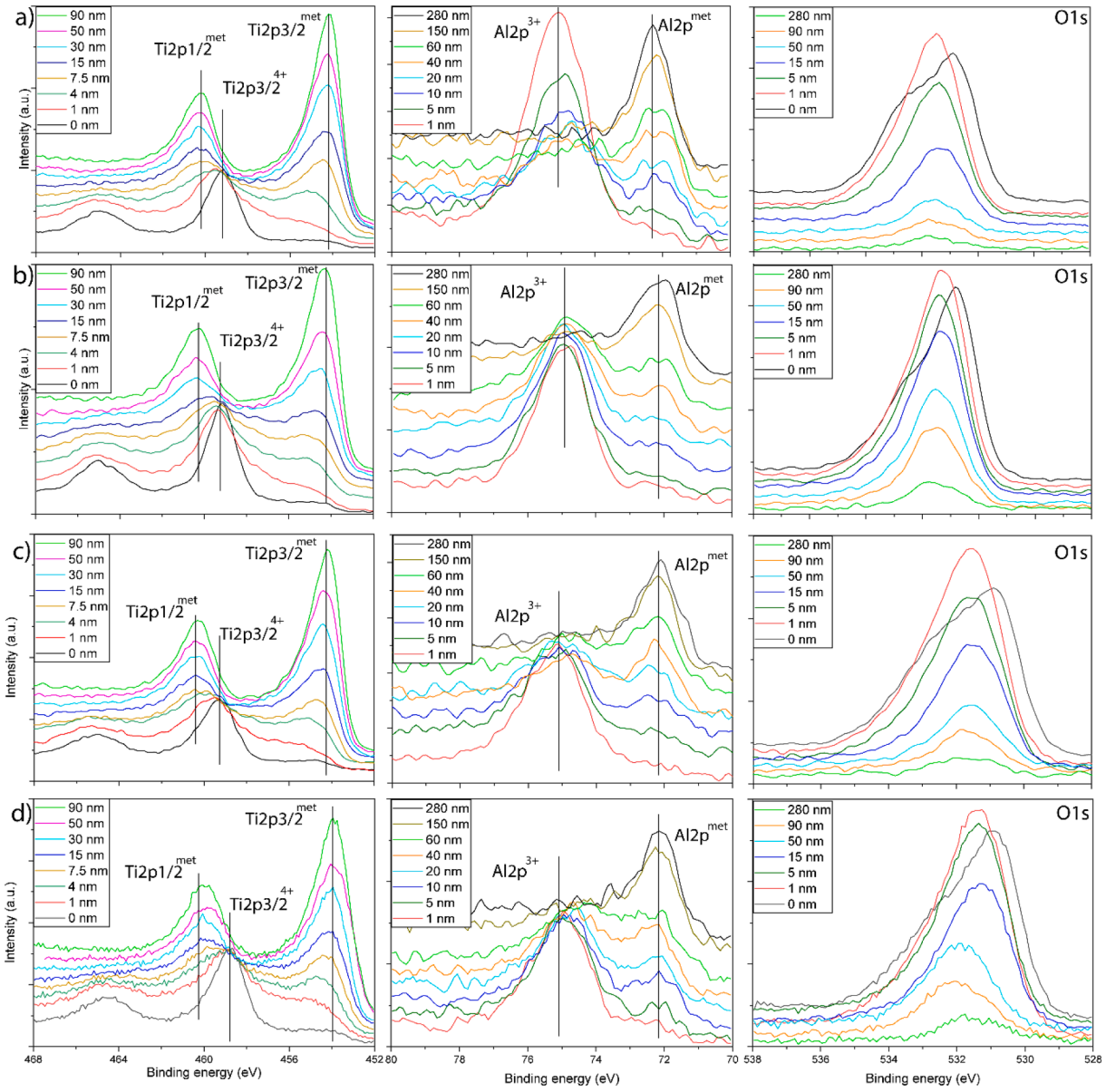


**Fig. 7.** A comparison of the depth profile of Ti2p, Al2p and O1s narrow spectra of a) virgin powder, and of spatters produced under b) Ar, c) Ar-He mixture, and d) He.

spatters compared to pure Ar atmosphere. This is perhaps connected to the higher cooling rate and specific heat capacity in the He atmosphere compared to Ar atmosphere which doesn't allow the spatters enough time to oxidize to similar extent as the spatters in Ar environment.

### 3.3.2. *Oxide composition and distribution*

Considering the presence of variation in surface oxide morphology on spatter particles, it is important to do point analysis on individual particles to investigate the composition and distribution of the oxide species with higher spatial resolution, that is typically done by Auger Electron Spectroscopy, allowing to reach spatial resolution down to 10 nm with the surface sensitivity up to 10 nm in depth. Fig. 10 is presenting an AES analysis where a comparison between virgin and oxidized spatter particles is shown. The virgin particle (Particle a) has a clean surface with a clear dendritic structure over the surface. The AES spectra of the virgin particle are mainly showing the presence of titanium peaks along with oxygen and carbon peaks. A peak from aluminium with minimal intensity is also present at 1370 eV, which indicates that the oxide layer on the surface of virgin particles mainly consists of Ti-based oxide with a minor contribution from Al. Contrarily, the surface of the oxidized spatter particle is covered with a uniform oxide particulate scale, see Fig. 10b. AES survey spectra from the area highlighted in the yellow square show the presence of strong Al peaks beside Ti, O, and C peaks, which were present in the virgin sample too. A strong Al peak in spectra from spatter particles is indicating the enrichment of Al on the particle surface. Hence, an assumption can be made that the oxide particulates on the surface of oxidized spatters are mainly connected to enrichment in Al along with the presence of Ti, whereas the oxide layer over the surface of virgin particles mainly consists of Ti-based oxide with a small contribution from Al.

A comparison of spatter particles' surface morphology, shown in Fig. 4, indicated that the spatter particles have three variations in terms of morphology. The chemistry and nature of oxides on these particles can significantly vary from each other. To investigate the variation, an AES depth profile analysis has been conducted on three different spatter particles, shown in Fig. 11. Fig. 11a shows a particle with virgin-like morphology where the surface is free of any oxide particulates with a lucid dendritic structure originating from the atomization. The AES

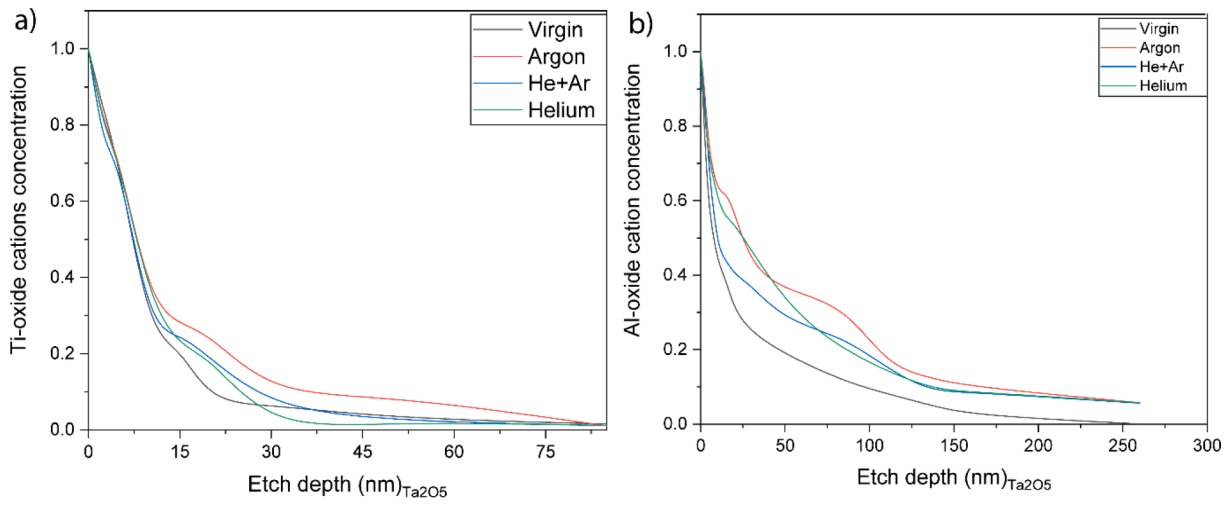


**Fig. 8.** Comparison of a) Ti-oxide cations and b) Al-oxide cations w.r.t. etch depth of virgin powder, and spatters produced under Ar, the *ADDvance® Laser230*, and He.

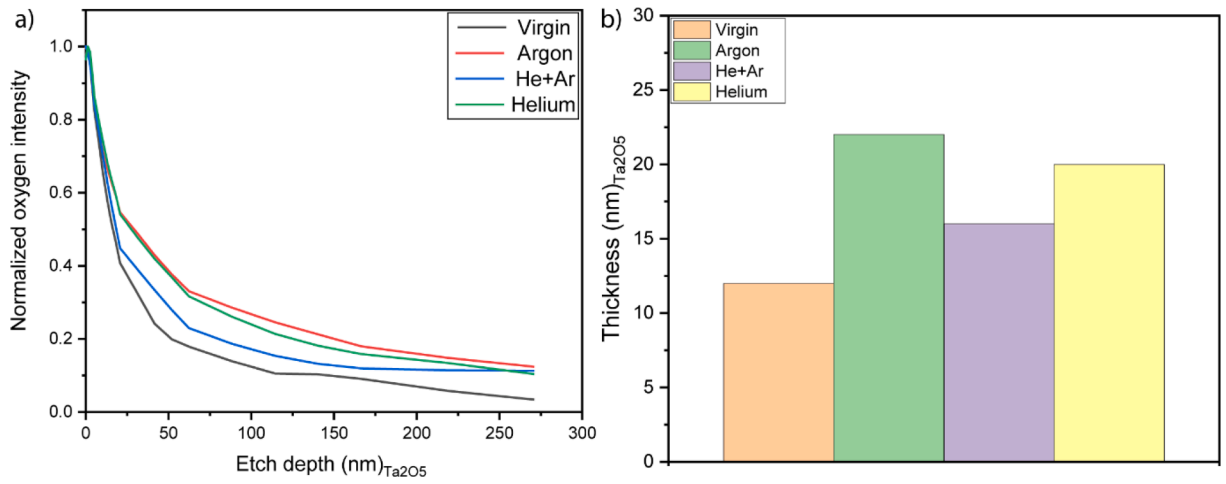


**Fig. 9.** Oxide layer thickness estimation from the normalized intensity of oxygen (O1s) for a) the virgin powder, and spatters produced under b) Ar, c)Ar-He, and d) He.

depth profile analysis of this particle shows (see Fig. 11d) a thin and uniform oxide layer formation on the top surface. A slight etching of the surface removed the oxide layer and exposed the inner metallic layer. Fig. 11b represents the group of recrystallized large spatters with a visible fine martensitic substructure on the surface along with small oxide nuclei. In the depth profile analysis by AES, a small plateau of oxygen can be observed right underneath the top oxide surface. This is an indication of the presence of oxide species at a larger depth than the virgin-like particle. Lastly, Fig. 11c shows an oxidized spatter particle where the surface of the particle is covered with thick oxide particulates. The AES depth profile shown in Fig. 11f confirms the oxidized nature of particulates on the surface. A large plateau with higher O and Al levels and lower Ti levels can be observed over the surface to the depth of 80 nm as per etch rate calibrated using $Ta_2O_5$ foil. After further ion-etching, a sudden decrease in the content of O and an increase in Ti content can be observed. This is an indication of interface between the particulates are Ti and Al-based oxides and metallic phases. To summarize the depth profile AES analysis on spatter particles, virgin-like particles are probably the entrapped by the processing gas virgin particles which are unaffected by laser -powder interaction and have the lowest oxide layer thickness followed by recrystallized spatter particles and oxidized spatter particles, respectively.

To better understand the composition of oxides, NanoSIMS was used to evaluate the mixed nature of oxide by measuring concentration maps on the powder particle surface. Fig. 12 is showing a comparison of the depth profile of concentration maps of fresh and spatter powders. The intensity of the maps is concentrated in the center of the particle which relates to the shadowing effect by the spherical shape of the powder particles. The concentration maps from fresh powder are showing the higher intensity of Ti-rich oxides as compared to the Al-rich oxide. With the slight etching of the surface, the oxide layer got depleted which is elucidated by the decrease in intensity of the oxides. This is an indication of low oxide layer thickness on the fresh powder surface as determined by other surface analysis techniques presented in this article. The persistence of signals with etching and overlapping of Ti and Al-based oxide signals is highlighting the enrichment in a localized region.

For spatter powders, the trend of oxide distribution is rather contradictory to the fresh powder where the surface oxide layer is significantly more enriched in Al-oxide with the presence of Ti-oxide at the same locations. On some sites, both types of oxide are overlapping which is connected to the mixed nature of oxides on the surface of spatter particles. This is an interesting finding by NanoSIMS analysis that the oxide scale has a mixed nature rather than forming the individual complex spinel-type oxide in localized regions. Such mixed nature originated from the high cooling rate of the spatter and lack of ample time, which has already been established for the spatters from alloy 718

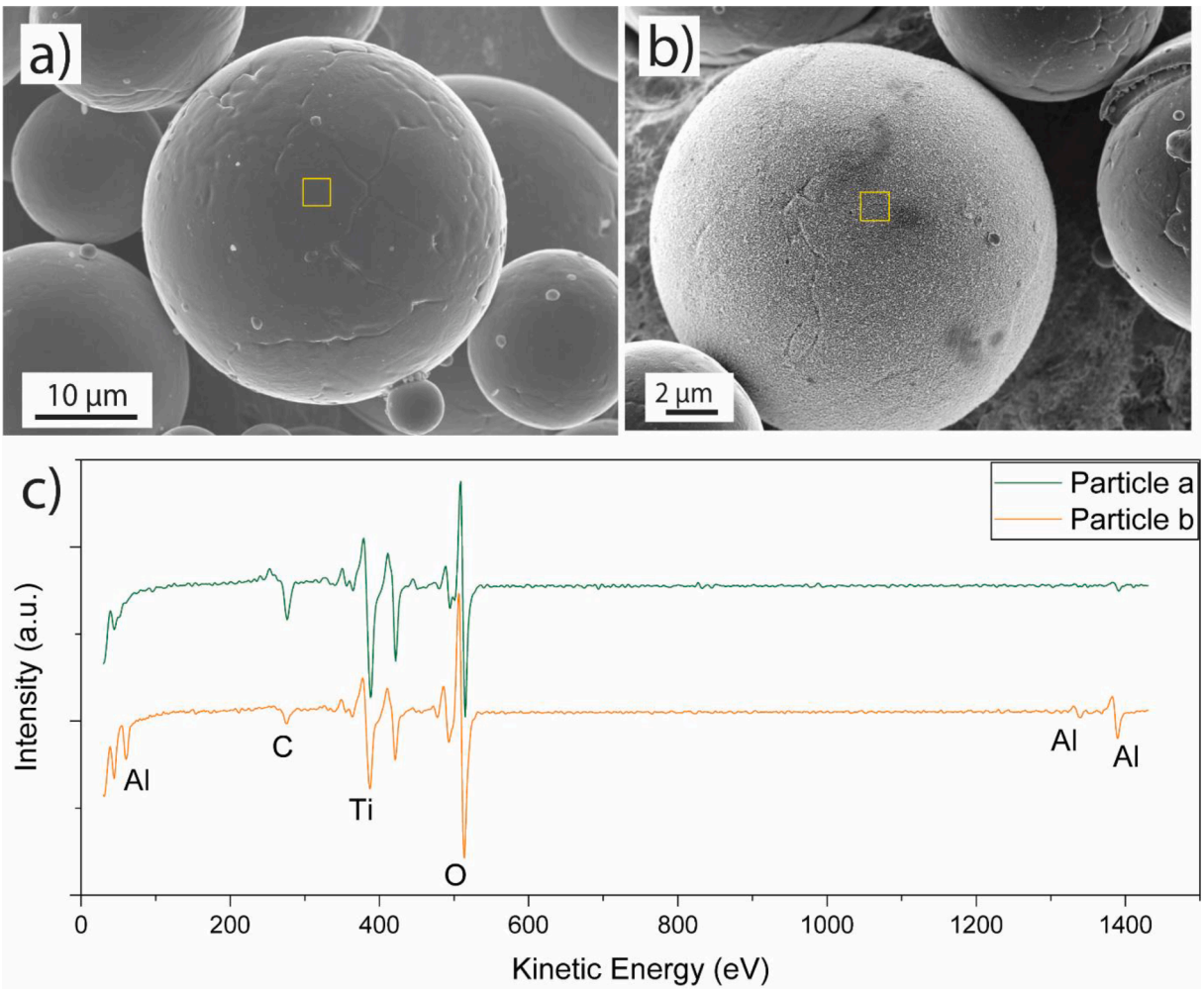


**Fig. 10.** A comparison of an AES analysis conducted on a) virgin and b) oxidized spatter particle with c) AES survey spectra highlighting the variation in surface concentrations.

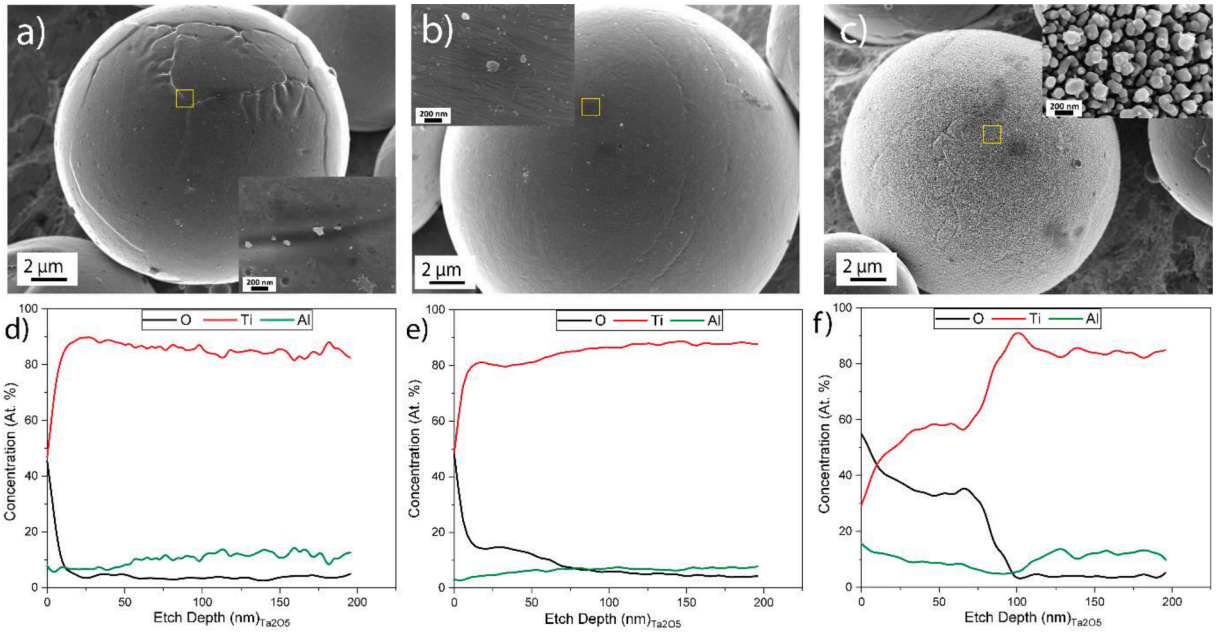


**Fig. 11.** A comparison of a) virgin-like, b) recrystallized, and c) oxidized spatter particles with AES depth profile presented in d), e) and f) respectively.

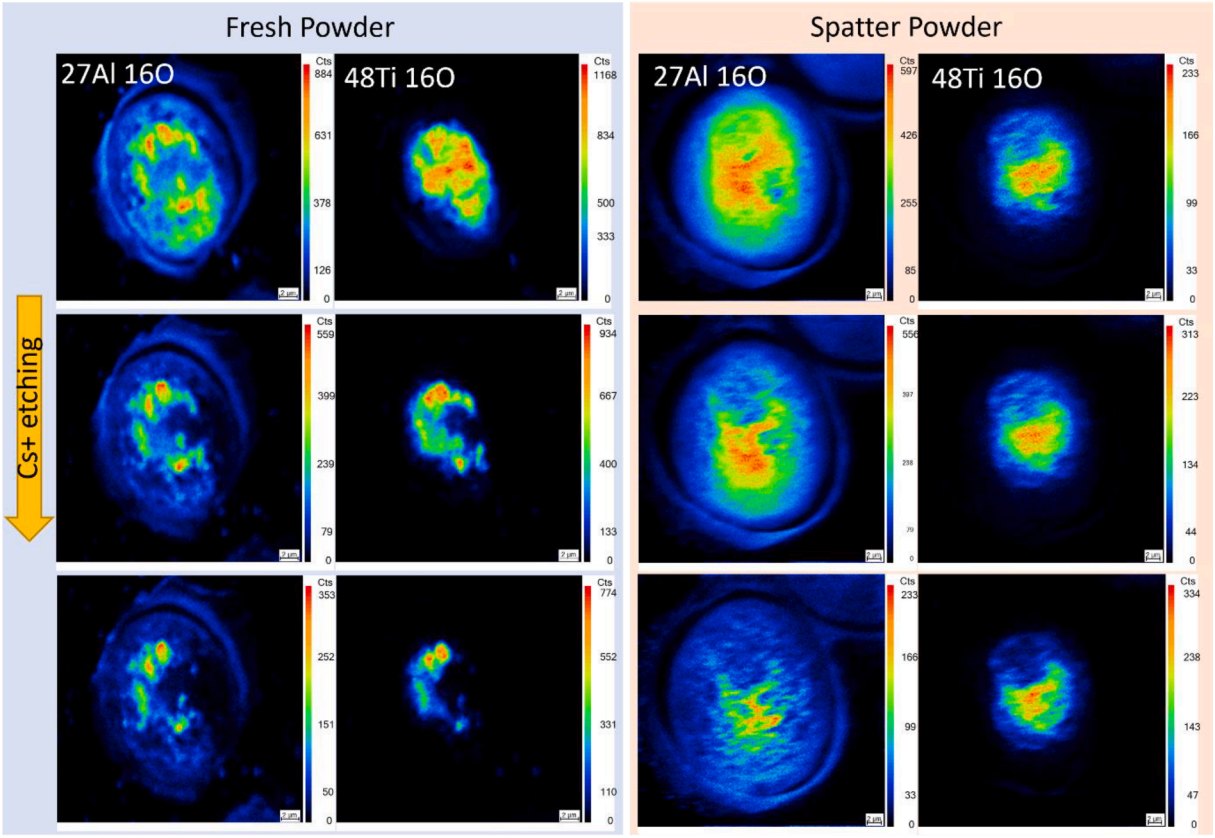


**Fig. 12.** NanoSIMS concentration maps for 27Al16O and 48Ti16O for fresh powder and spatters powders where the concentration maps are compared at different etched depths.

and AlSi10Mg alloy in our previous studies [15,23].

## 4. Conclusions

This study analyses the effect of atmospheric gas on spatter generation and oxidation during PBF-LB processing of TiAl6V4 by comprehensive surface analysis. There are several conclusions which can be drawn from this study which can be summarised as follows:

- Introduction of He in the built atmosphere reduced the amount of generated spatters up to 30 % in the *ADDvance® Laser230* atmosphere compared to pure argon.
- The bulk chemical analysis by combustion showed the highest increase in oxygen (70%), hydrogen (300%), and nitrogen (>300%) in the spatter particles collected in argon followed by argon-helium and helium. The samples collected in Ar/He mixture and He had a similar pickup of oxygen. Perhaps this relates to the thermal conductivity of He gas which is higher than argon. The higher conductivity of helium assisted in faster cooling of spatters which limited the time of oxidation.
- Comparison of the morphology of spatters with virgin powder showed the formation of oxide particulates on the spatter surface which were not present on the virgin particles. The spatter particles also oxidized differently where the surface of some spatters possessed granular oxide scale on the surface.
- XPS analysis showed that the oxide scale predominantly consisted of Al-enriched and Ti-based oxide layers. The thickness of Al-rich oxide was thicker than the uniform oxide layer, indicating the formation of Al-rich oxide particulates.
- The average oxide layer thickness measured through XPS analysis also showed that the oxide layer thickness almost doubled from virgin to spatters collected in the argon atmosphere from ~7.2 nm for the virgin powder to about ~13.5 nm, ~11 nm, and 12 nm for the spatters sampled during PBF-LB processing in Ar, Ar-He and He, respectively.
- The AES analysis showed that the spatters have different extent of oxidation depending upon the origin of the spatters and nature of their interaction with the laser and melt pool. AES analysis confirmed that granular oxides, forming oxide scale on the spatters, consists of mixed Al-Ti-oxides.
- The NanoSIMS analysis confirms that the virgin powder is covered with a thin oxide layer consisted of Ti-based oxide with some presence of Al-oxide, whereas the spatters have significantly higher enrichment in Al-oxide. Overlap between Al- and Ti-based oxides indicate presence of the mixed oxides.

This study suggests that the processing gas strongly influences the amount of generated spatters and the extent of oxidation. Owing to the higher thermal conductivity of helium gas, the introduction of helium gas in the atmosphere can substantially reduce the number of generated spatters as well as the extent of spatter oxidation. Based on the detrimental role of spatters in powder reusability, this has significant impact on the improvement of the reusability of powder, and hence allows to reduce the cost, increase the robustness and sustainability of the PBF-LB process.

*CRediT authorship contribution statement*

**Ahmad Raza:** Conceptualization, Methodology, Investigation, Formal analysis, Visualization, Writing – original draft. **Camille Pauzon:** Conceptualization, Investigation, Formal analysis, Writing – original draft. **Sophie Dubiez-Le Goff:** Resources, Supervision, Writing – review & editing. **Eduard Hryha:** Conceptualization, Methodology, Funding acquisition, Project administration, Supervision.

## Declaration of Competing Interest

The authors declare that they have no known competing financial interests or personal relationships that could have appeared to influence the work reported in this paper.

## Data availability

Data will be made available on request.

## Acknowledgement

This work was conducted in the framework of the Centre for Additive Manufacturing – Metal (CAM$^2$) supported by the Swedish Governmental Agency of Innovation Systems (Vinnova). The authors would also like to acknowledge Katri Kakko (EOS) for her assistance with condensation analysis. NanoSIMS measurements were performed at the Infrastructure for Chemical imaging at Chalmers University of Technology/University of Gothenburg.

## References

[1] P. Moghimian, T. Poirié, M. Habibnejad-Korayem, J.A. Zavala, J. Kroeger, F. Marion, F. Larouche, Metal powders in additive manufacturing: A review on reusability and recyclability of common titanium, nickel and aluminum alloys, Addit. Manuf. 43 (2021) 102017.

[2] A. Montelione, S. Ghods, R. Schur, C. Wisdom, D. Arola, M. Ramulu, Powder Reuse in Electron Beam Melting Additive Manufacturing of Ti6Al4V: Particle Microstructure, Oxygen Content and Mechanical Properties, Addit. Manuf. 35 (2020), 101216, https://doi.org/10.1016/j.addma.2020.101216.

[3] E. Hryha, R. Shvab, H. Gruber, A. Leicht, L. Nyborg, Surface oxide state on metal powder and its changes during additive manufacturing: An overview, in: Proc. Euro PM 2017 Int. Powder Metall. Congr. Exhib., 2018.

[4] J. Yin, L.L. Yang, X. Yang, H. Zhu, D. Wang, L. Ke, Z. Wang, G. Wang, X. Zeng, High-power laser-matter interaction during laser powder bed fusion, Addit. Manuf. 29 (2019), 100778, https://doi.org/10.1016/j.addma.2019.100778.

[5] P. Deng, M. Karadge, R.B. Rebak, V.K. Gupta, B.C. Prorok, X. Lou, The origin and formation of oxygen inclusions in austenitic stainless steels manufactured by laser powder bed fusion, Addit. Manuf. 35 (2020), 101334, https://doi.org/10.1016/j.addma.2020.101334.

[6] D. Powell, A.E.W. Rennie, L. Geekie, N. Burns, Understanding powder degradation in metal additive manufacturing to allow the upcycling of recycled powders, J. Clean. Prod. 268 (2020), 122077, https://doi.org/10.1016/j.jclepro.2020.122077.

[7] E. Santecchia, S. Spigarelli, M. Cabibbo, Material reuse in laser powder bed fusion: Side effects of the laser—metal powder interaction, Metals (Basel) 10 (2020) 1–21, https://doi.org/10.3390/met10030341.

[8] S.A. Khairallah, A.T. Anderson, A. Rubenchik, W.E. King, Laser powder-bed fusion additive manufacturing: Physics of complex melt flow and formation mechanisms of pores, spatter, and denudation zones, Acta Mater. 108 (2016) 36–45, https://doi.org/10.1016/j.actamat.2016.02.014.

[9] A.N.D. Gasper, D. Hickman, I. Ashcroft, S. Sharma, X. Wang, B. Szost, D. Johns, A. T. Clare, Oxide and spatter powder formation during laser powder bed fusion of Hastelloy X, Powder Technol. 354 (2019) 333–337, https://doi.org/10.1016/j.powtec.2019.06.004.

[10] Z.A. Young, Q. Guo, N.D. Parab, C. Zhao, M. Qu, L.I. Escano, K. Fezzaa, W. Everhart, T. Sun, L. Chen, Types of spatter and their features and formation mechanisms in laser powder bed fusion additive manufacturing process, Addit. Manuf. 36 (2020), 101438, https://doi.org/10.1016/j.addma.2020.101438.

[11] C. Pauzon, A. Raza, E. Hryha, P. Forêt, Oxygen balance during laser powder bed fusion of Alloy 718, Mater. Des. 201 (2021), https://doi.org/10.1016/j.matdes.2021.109511.

[12] C.L.A. Leung, S. Marussi, M. Towrie, R.C. Atwood, P.J. Withers, P.D. Lee, The effect of powder oxidation on defect formation in laser additive manufacturing, Acta Mater. 166 (2019) 294–305, https://doi.org/10.1016/j.actamat.2018.12.027.

[13] A.N.D. Gasper, B. Szost, X. Wang, D. Johns, S. Sharma, A.T. Clare, I.A. Ashcroft, Spatter and oxide formation in laser powder bed fusion of Inconel 718, Addit. Manuf. 24 (2018) 446–456, https://doi.org/10.1016/j.addma.2018.09.032.

[14] F. Ahmed, U. Ali, D. Sarker, E. Marzbanrad, K. Choi, Y. Mahmoodkhani, E. Toyserkani, Study of powder recycling and its effect on printed parts during laser powder-bed fusion of 17–4 PH stainless steel, J. Mater. Process. Technol. 278 (2020), 116522, https://doi.org/10.1016/j.jmatprotec.2019.116522.

[15] A. Raza, T. Fiegl, I. Hanif, A. Markström, M. Franke, C. Körner, E. Hryha, Degradation of AlSi10Mg powder during laser based powder bed fusion processing, Mater. Des. 198 (2021), 109358, https://doi.org/10.1016/j.matdes.2020.109358.

[16] T. Fiegl, M. Franke, A. Raza, E. Hryha, C. Körner, Effect of AlSi10Mg0.4 long-term reused powder in PBF-LB/M on the mechanical properties, Mater. Des. 212 (2021), 110176, https://doi.org/10.1016/j.matdes.2021.110176.

[17] U. Ali, R. Esmaeilizadeh, F. Ahmed, D. Sarker, W. Muhammad, A. Keshavarzkermani, Y. Mahmoodkhani, E. Marzbanrad, E. Toyserkani, Identification and characterization of spatter particles and their effect on surface roughness, density and mechanical response of 17–4 PH stainless steel laser powder-bed fusion parts, Mater. Sci. Eng. A. 756 (2019) 98–107, https://doi.org/10.1016/j.msea.2019.04.026.

[18] C. Schwerz, A. Raza, X. Lei, L. Nyborg, E. Hryha, H. Wirdelius, In-situ detection of redeposited spatter and its influence on the formation of internal flaws in laser powder bed fusion, Addit. Manuf. 47 (2021), 102370, https://doi.org/10.1016/j.addma.2021.102370.

[19] M. Slodczyk, A. Ilin, T. Kiedrowski, T. Bareth, V. Ploshikhin, Spatter reduction by multi-beam illumination in laser powder-bed fusion, Mater. Des. 212 (2021), 110206, https://doi.org/10.1016/j.matdes.2021.110206.

[20] M. Taheri Andani, R. Dehghani, M.R. Karamooz-Ravari, R. Mirzaeifar, J. Ni, A study on the effect of energy input on spatter particles creation during selective laser melting process, Addit. Manuf. 20 (2018) 33–43, https://doi.org/10.1016/j.addma.2017.12.009.

[21] V. Gunenthiram, P. Peyre, M. Schneider, M. Dal, F. Coste, I. Koutiri, R. Fabbro, Experimental analysis of spatter generation and melt-pool behavior during the powder bed laser beam melting process, J. Mater. Process. Technol. 251 (2018) 376–386, https://doi.org/10.1016/j.jmatprotec.2017.08.012.

[22] Z. Chen, A. Raza, E. Hryha, Influence of part geometry on spatter formation in laser powder bed fusion of Inconel 718 alloy revealed by optical tomography, J. Manuf. Process. 81 (2022) 680–695, https://doi.org/10.1016/j.jmapro.2022.07.031.

[23] A. Raza, C. Pauzon, E. Hryha, A. Markström, P. Forêt, Spatter oxidation during laser powder bed fusion of Alloy 718: dependence on oxygen content in the process atmosphere, Addit. Manuf. 48 (2021), 102369, https://doi.org/10.1016/j.addma.2021.102369.

[24] H. Amano, Y. Yamaguchi, T. Ishimoto, T. Nakano, Reduction of spatter generation using atmospheric gas in laser powder bed fusion of Ti6Al4V, Mater. Trans. 62 (2021) 1225–1230, https://doi.org/10.2320/matertrans.MT-M2021059.

[25] S. Traore, M. Schneider, I. Koutiri, F. Coste, R. Fabbro, C. Charpentier, P. Lefebvre, P. Peyre, Influence of gas atmosphere (Ar or He) on the laser powder bed fusion of a Ni-based alloy, J. Mater. Process. Technol. 288 (2021), 116851, https://doi.org/10.1016/j.jmatprotec.2020.116851.

[26] C. Pauzon, B. Hoppe, T. Pichler, S. Dubiez-Le Goff, P. Forêt, T. Nguyen, E. Hryha, Reduction of incandescent spatter with helium addition to the process gas during laser powder bed fusion of Ti-6Al-4V, CIRP J. Manuf. Sci. Technol. 35 (2021) 371–378, https://doi.org/10.1016/j.cirpj.2021.07.004.

[27] Z. Li, H. Li, J. Yin, Y. Li, Z. Nie, X. Li, D. You, K. Guan, W. Duan, L. Cao, D. Wang, L. Ke, Y. Liu, P. Zhao, L. Wang, K. Zhu, Z. Zhang, L. Gao, L. Hao, A Review of Spatter in Laser Powder Bed Fusion Additive Manufacturing: In Situ Detection, Generation, Effects, and Countermeasures, Micromachines 13 (8) (2022) 1366.

[28] C. Pauzon, T. Mishurova, S. Evsevleev, S. Dubiez-Le Goff, S. Murugesan, G. Bruno, E. Hryha, Residual stresses and porosity in Ti-6Al-4V produced by laser powder bed fusion as a function of process atmosphere and component design, Addit. Manuf. 47 (2021), 102340, https://doi.org/10.1016/j.addma.2021.102340.

[29] L. Nyborg, A. Nylund, I. Olefjord, Thickness determination of oxide layers on spherically-shaped metal powders by ESCA, Surf. Interface Anal. 12 (2) (1988) 110–114.

[30] C. Oikonomou, D. Nikas, E. Hryha, L. Nyborg, Evaluation of the thickness and roughness of homogeneous surface layers on spherical and irregular powder particles, Surf. Interface Anal. 46 (2014) 1028–1032, https://doi.org/10.1002/sia.5439.

[31] D.R. Baer, M.H. Engelhard, A.S. Lea, P. Nachimuthu, T.C. Droubay, J. Kim, B. Lee, C. Mathews, R.L. Opila, L.V. Saraf, W.F. Stickle, R.M. Wallace, B.S. Wright, Comparison of the sputter rates of oxide films relative to the sputter rate of $SiO_2$, J. Vac. Sci. Technol. A Vacuum, Surfaces, Film 28 (2010) 1060–1072, https://doi.org/10.1116/1.3456123.